J. Min. Metall. Sect. B-Metall. 55 (3) B (2019) 397 - 404

Journal of Mining and Metallurgy, Section B: Metallurgy

EFFECT OF CaF_2 SUBSTITUTION WITH TiO_2 ON THE CRYSTALLIZATION CHARACTERISTICS OF LOW-FLUORIDE SLAG FOR ELECTROSLAG REMELTING

J.-T. Ju *, J.-L An, G.-H. Ji

School of Metallurgical Engineering, Xi'an University of Architecture and Technology, Xi'an, China

(Received 15 February 2019; accepted 20 May 2019)

Abstract

The effect of CaF_2 substitution with TiO_2 on the crystallization characteristics of low-fluoride slag was studied using differential scanning calorimetry (DSC) combined with XRD and SEM-EDS analysis. The effective activation energy for crystallization of the slag was evaluated. The results showed that the liquidus temperature of the slag increased unnoticeably with increasing TiO_2 content. Increasing TiO_2 addition from 4.3 wt% to 13.0 wt% decreased the undercooling of the slag and enhanced the crystallization ability of the slag. There is no change in the types and precipitation sequence of the crystalline phase in the slag with different TiO_2 contents during continuous cooling. The crystalline phases were $Ca_{12}Al_{14}O_{32}F_2$, $CaTiO_3$, MgO, and CaF_2. The first and second crystallization phase were $Ca_{12}Al_{14}O_{32}F_2$ and $CaTiO_3$, respectively. The dominant crystalline phase was faceted $Ca_{12}Al_{14}O_{32}F_2$ crystals. The morphology of $CaTiO_3$ crystal changed from needle-like to blocky with increasing TiO_2 content. The MgO crystal was with little blocky morphology, and the needle-like CaF_2 distributed among $CaTiO_3$ crystal. The precipitated amount of both MgO and CaF_2 was very small. The effective activation energy for $Ca_{12}Al_{14}O_{32}F_2$ formation decreased with increasing TiO_2 content in the slag, indicating that TiO_2 enhanced the crystallization tendency of the slag.

Keywords: *Crystallization characteristics; Low-fluoride slag; TiO_2; Electroslag remelting; Effective activation energy for crystallization*

1. Introduction

Electroslag remelting (ESR) allows a good control of the cleanliness and solidification structure of the ingot [1]. Slag plays an important role in the ESR process, including generating Joule heat for melting electrode, removing harmful elements and non-metallic inclusions, *etc* [2-4]. The ESR slag contains a large amount of fluoride, such as 70%CaF_2-30%$A1_2O_3$, 60%CaF_2-20%CaO-20%$A1_2O_3$, 40%CaF_2-30%CaO-30%$A1_2O_3$, *etc.*, in order to decrease melting temperature and viscosity of the slag. However, the volatilization of fluoride from molten slag melt during ESR process has always been a big obstacle because it causes environmental pollution, corrosion of plant equipment, and the chemical composition change of the slag [5-6]. Furthermore, the chemistry change of slag caused by volatilization of fluoride generally reduces the stability of operating practice and degrade the quality of as-ingot [7].

Only a few studies regarding the development of low-fluorine or fluorine-free ESR slag have been reported. Narita *et al.*[8] investigated the application of CaO-Al_2O_3-based slag in ESR, and found that there was no trouble during the operation when using CaO-Al_2O_3-based slags with no fuming and good electric stability. Liang *et al.*[9] showed that the power consumption could decrease about 30% by using 49.5%CaO-43.7%Al_2O_3-6.8%SiO_2 slag and 52.0%CaO-41.2%Al_2O_3-6.8%SiO_2 in comparison to 60%CaF_2-20%CaO-20%$A1_2O_3$ slag, and reduce fluoride pollution as well. Mao *et al.*[10] reported that the CaO-Al_2O_3-MgO fluorine-free slag can guarantee the quality of G20CrNi2MoA as-ingot and improve environmental pollution. Rehak *et al.*[11] found that using fluorine-free CaO-Al_2O_3 slag in the ESR production of Al-killed steel could decrease the amount of oxide inclusions. Although several applications of low-fluorine and fluorine-free ESR slag have been performed in industrial trial, the widely used ESR slag is still high-fluorine slag which has not been completely substituted by low-fluorine or fluorine-free ESR slag. This is because the application of these slags still generates several problems, such as the difficulties in liquid slag starting, controlling of the as-cast surface quality and high working voltage, etc., which

**Corresponding author: ju_jiantao@163.com*

https://doi.org/10.2298/JMMB190215034J

is strongly dependent on the thermo-physical properties of the slag [12,13].

The main idea for the development of low-fluorine or fluorine-free ESR slag was to control the CaO/Al_2O_3 ratio and substitute a small amount of MgO or SiO_2 for CaF_2. In the ESR production of Ti-containing steel and alloy, TiO_2 is always added to the ESR slag to minimize the titanium loss [14,15]. Many researches on the low-fluorine and fluorine-free metallurgical slag suggested that TiO_2 has the similar effect as CaF_2 on the thermo-physical properties of the slag, such as reducing the viscosity and increasing electrical conductivity of slag [16-18]. Moreover, TiO_2 is more difficult to volatilize than CaF_2. It provides guidance to develop low-fluorine ESR slag by substituting TiO_2 for CaF_2 in the ESR production of Ti-containing steel and alloy.

The previous studies [19-21] demonstrated that the crystallization characteristic of ESR slag was a vital factor in determining the current distribution in mold and surface quality of as-cast ingot. The present work was carried out to study the influence of substitution of CaF_2 with TiO_2 on the crystallization characteristic of low-fluoride ESR slag. The differential scanning calorimetry (DSC) was employed to study the crystallization behavior of the slag. Continuous cooling transformation (CCT) diagrams of crystalline phases were plotted based on the DSC curves. The types and morphology of the crystalline phases were identified by XRD and SEM-EDS analysis. In addition, the effective activation energy for crystallization of the slag was evaluated based on DSC thermal data.

2. Experimental

2.1 Sample Preparation

Slag samples were prepared using reagent-grade powders of CaF_2, $CaCO_3$, Al_2O_3, MgO, Li_2CO_3, and TiO_2 powder. $CaCO_3$ powder was calcined at 1323 K for 10 h in muffle furnace to produce CaO. The thoroughly mixed powder was pre-melted at 1773 K (1500 °C) in a platinum crucible for 5 min, and subsequently the liquid sample was quenched in iced water and crushed. The chemical composition of the slag was analyzed using inductively coupled plasma-optical emission spectroscopy. The fluorine content of pre-melted slag was determined by ion-selective electrode method. The chemical composition of the pre-melted slag is shown in Table 1.

Table 1. *Chemical composition of the pre-melted slag /wt%*

Sample No.	CaF_2	CaO	Al_2O_3	MgO	Li_2O	TiO_2
A	16.4	38.7	35.6	2.4	2.6	4.3
B	15.8	37.5	33.1	2.4	2.6	8.6
C	13.6	37.4	31.4	2.4	2.2	13

2.2 DSC Measurement

The crystallization characteristics of the slag were investigated by DSC (Netzsch STA449F3; Netzsch Instrument Inc., Germany) measurements in Ar gas atmosphere at a flow rate of 70 mL/min. For each DSC measurement, approximately 50 mg of sample was heated at the heating rate of 30 K/min from room temperature up to 1773 K (1500 °C) in a platinum crucible and held for 1 min to eliminate bubbles and homogenize its chemical composition. Then, the liquid sample was cooled at a constant cooling rate (10 K/min, 15 K/min, 20 K/min and 25 K/min) to the room temperature.

2.3 SEM-EDS and XRD analysis

The slag samples after DSC measurements were mounted with epoxy resin and polished. Then, a thin platinum film was coated onto the cross section of the polished sample to enhance the sample electric conductivity. The morphology and composition of crystalline phases in slag samples after DSC measurements were determined by the SEM-EDS analysis.

Considering that the slag samples after DSC measurements were too small to determine crystalline phase by XRD analysis, a series of cooling experiments were carried out to determine the types of the crystalline phases in slag samples corresponding to each exothermic peak of the DSC curves. Approximately 2 g of slag was put in a platinum crucible at 1773 K (1500 °C) for 1 minute, then cooled at the cooling rate of 10 K/min to the target temperature and held for 1 h. The slag sample was quenched by ice water and the crystalline phases in the slag were analyzed by the XRD analysis.

3. Results and Discussion

3.1 DSC Measurement and XRD Identification

Figure 1 shows the DSC curves of the slag at four different cooling rates, i.e., 10 K/min, 15 K/min, 20 K/min, and 25 K/min, respectively. The exothermic peak on DSC curves indicates the crystalline phase formation event. Four exothermic peaks are observed on the DSC curves of the three slag samples at various cooling rates, which are designated as P1, P2, P3, and P4, respectively. It should be noted that the intensity of P3 and P4 on the DSC curves are much lower than those of P1 and P2 that the peaks are difficult to detect on the DSC curves, especially in Figure 1(a) and Figure 1(c). It could be because that the precipitated amount of the crystalline phases corresponding to both P3 and P4 are very small,

which can be verified by the SEM-EDS results of the slag samples (presented in section 3.3) after the DSC measurements. Figure 1(b) shows that the third exothermic peak overlaps partially with the fourth exothermic peak at various cooling rates, indicating that the crystalline phase corresponding to P4 started to precipitate before the finish of the crystalline phase formation corresponding to P3. Furthermore, the intensity of first exothermic peak is much higher than the other three exothermic peaks for the three slag samples at various cooling rates, suggesting that the peak P1 should represent the dominate crystalline phase in the slag samples.

Figure 2 shows the XRD patterns of the slag samples quenched at the different temperatures. Four crystalline phases were identified at 1000 °C in each slag sample by XRD, *i.e.*, $Ca_{12}Al_{14}O_{32}F_2$, $CaTiO_3$, MgO, and CaF_2. There is no change in the types of the crystalline phase in the studied slag samples with different TiO_2 contents during continuous cooling. From Figure 2(c) to 2(e), the first and second exothermic peaks on the DSC curves for slag C represent the precipitation of $Ca_{12}Al_{14}O_{32}F_2$ and $CaTiO_3$ during the continuous cooling of the slag, respectively. The third exothermic peak and the fourth exothermic peak on the DSC curves represent the precipitation of MgO and CaF_2 for the three slag samples at various cooling rates. According to the morphology of the crystallization phase shown in Section 3.3, it can be deduced that increasing TiO_2 content from 4.3 wt% to 13.0 wt% in the slag has no influence on the precipitation sequence of the crystalline phase. Therefore, it was concluded that the first and second exothermic peaks on the DSC curves for the slag correspond to the precipitation of $Ca_{12}Al_{14}O_{32}F_2$ and $CaTiO_3$, respectively. It should be noted that the XRD peaks of MgO and CaF_2 are much weaker than those of $Ca_{12}Al_{14}O_{32}F_2$, $CaTiO_3$ in Figure 3(a) to 3(c). In consideration that the precipitated amount of the MgO and CaF_2 are much lower in the slag and the peak P3 overlaps partially with peak P4 in Figure 2(b), the XRD identification was not carried out to identify the precipitation order of MgO and CaF_2 in the slag.

3.2 Crystallization temperature and crystallization ability of the slag

The onset temperature of the exothermic peak on the DSC curve can be determined as the precipitation temperature of crystalline phase, at which the crystalline phase starts to precipitate [22]. Figure 3 shows the CCT diagrams of the crystalline phases in the slag constructed based on the records on the DSC curves at various cooling rates to clarify the crystallization tendency of the studied slag. It can be found that the precipitation temperatures of the crystalline phases in each slag decrease with increasing cooling rate due to stronger driving force needed to promote the nucleation in the molten slag with increasing the cooling rate [23,24]. Therefore, the precipitation temperature decreases with increasing cooling rate to provide larger undercooling for the nucleation.

Based on the DSC curves of the slag samples, the CCT diagrams for first and second crystalline phase in the slag samples were constructed, as shown in Figure 4. The precipitation temperature of the first crystalline phase during cooling process represents the crystallization temperature of the slag. It is clear from Figure 4(a) that the precipitation temperature of the first crystalline phase $Ca_{12}Al_{14}O_{32}F_2$ increases with increasing the TiO_2 content in slag, indicating that the addition of TiO_2 enhances the tendency of crystallization. As shown in Figure 4(b), the precipitation temperature of the second crystalline phase $CaTiO_3$ in slag A is much lower than those in slag B and slag C. And increasing TiO_2 content from

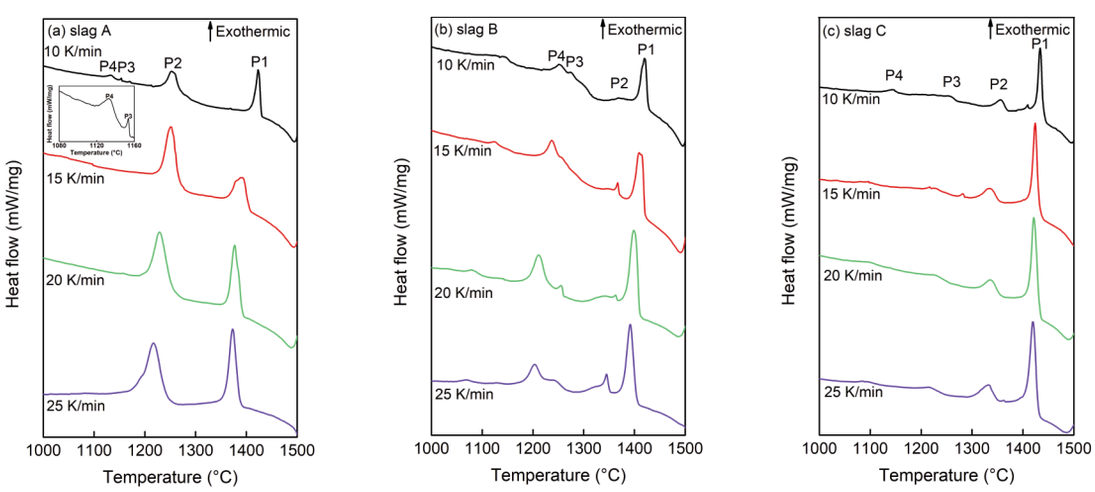

Figure 1. *DSC curves of the slag at various cooling rates*

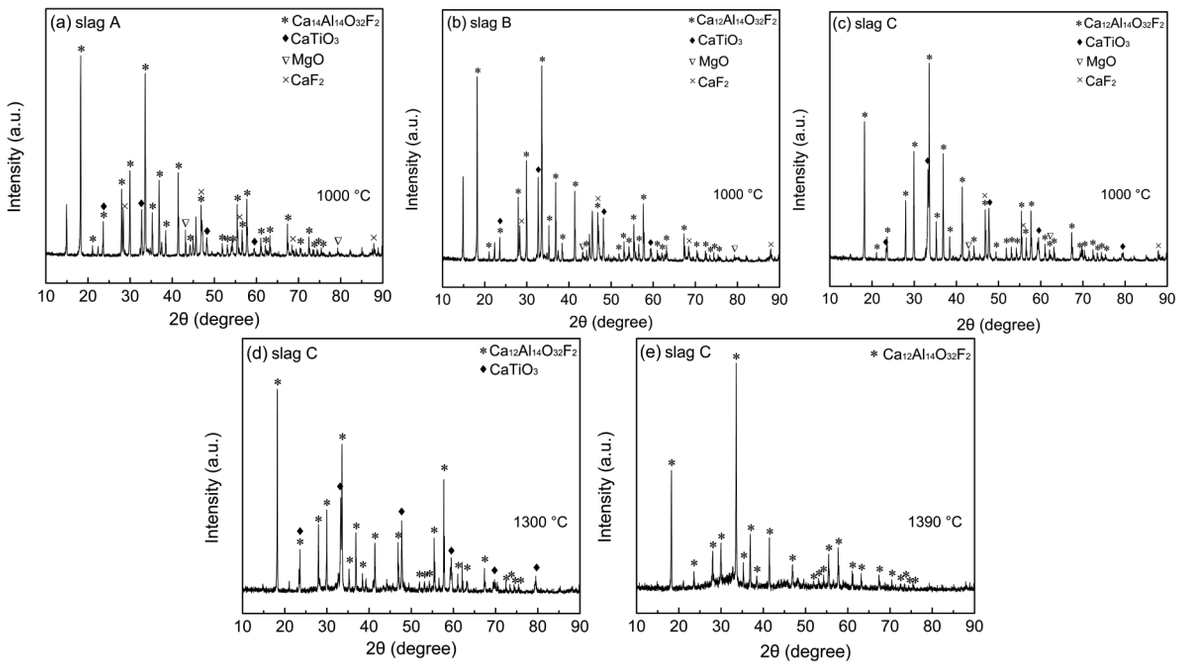

Figure 2. *XRD results of the slag quenched at various temperatures*

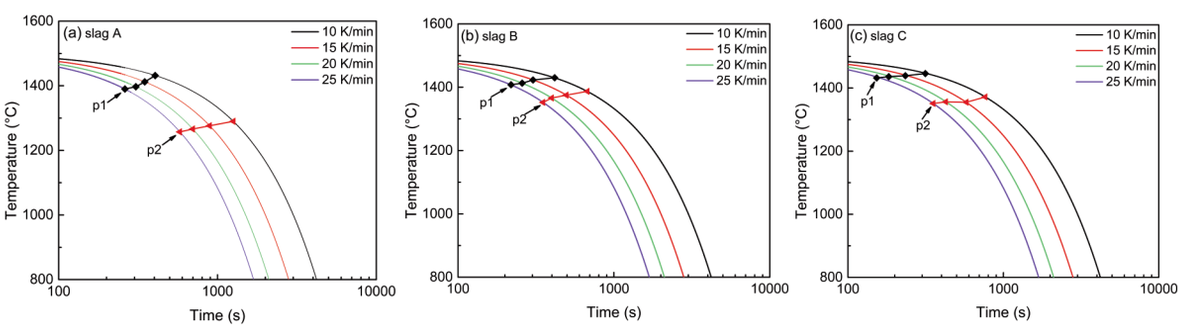

Figure 3. *CCT diagrams of the slag with various TiO_2 content*

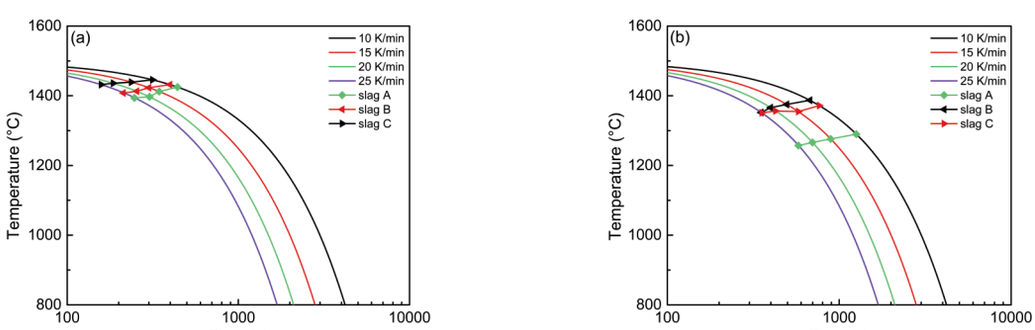

Figure 4. *CCT diagram of crystalline phase precipitated in the slag: (a) first crystalline phase $Ca_{12}Al_{14}O_{32}F_2$; (b) second crystalline phase $CaTiO_3$*

8.6 wt% to 13.0 wt% has no obvious effect on the precipitation temperature of $CaTiO_3$. This result is consistent with the finding reported by others [25]. The slag with a higher crystallization temperature easily forms a thick slag skin and unstable heat flux across the slag skin. In this case, it provides an unsound condition for the surface quality of remelted ingot [20,27]. Therefore, it is not suitable to substitute excessive TiO_2 for CaF_2 in the low-fluoride slag for electroslag remelting.

The liquidus temperature of slag is the temperature at which solid slag is completely transformed into liquid, which can be obtained by extrapolating the crystallization temperatures of slag at the various cooling rates to the value at the cooling rate of 0 K/min [20]. The extrapolated liquidus temperature of the studied slag is 1719 K (1446 °C), 1720 K (1447 °C), and 1727 K (1454 °C), respectively. It suggested that the increasing of the liquidus temperatures of the studied slag was not very noticeable with increasing TiO_2 addition. The undercooling can be applied to evaluate the crystallization ability of the slag. The calculated undercoolings of the slag at various cooling rates are presented in Figure 5. It is noted that the undercooling of slag decreases with increasing TiO_2 addition in the slag, indicating that the crystallization ability of the slag was enhanced with increasing TiO_2 content from 4.3 wt% to 13.0 wt% in the slag.

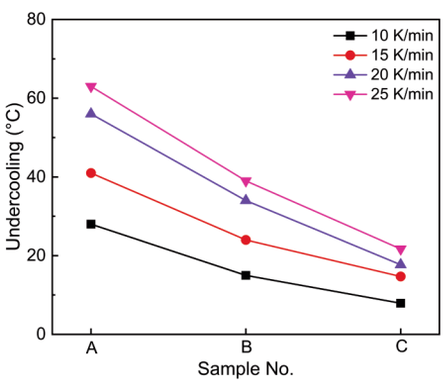

Figure 5. *Undercooling of the slag crystallization at various cooling rates*

3.3 SEM-EDS observation of the crystals in the slag

The morphologies and compositions of crystalline phases in the slag after DSC experiments were identified by SEM-EDS analysis. The types of the crystalline phases can be determined by combining the SEM-EDS with XRD results. Figures 6 to 9 show the SEM images of the slag after DSC measurements at the cooling rate of 10 K/min. Four crystalline phases were found in the slag, agreeing with DSC and XRD results. The element mappings of slag C shown in Figure 9 present the major element composition of the four crystalline phases. The dominant crystalline phase in the slag was faceted $Ca_{12}Al_{14}O_{32}F_2$ crystal, taking up most of the crystalline fraction in the slag, which suggested that the crystallization of $Ca_{12}Al_{14}O_{32}F_2$ crystal was controlled by interfacial reaction. Under this condition, viscosity had no vital influence on the crystallization of $Ca_{12}Al_{14}O_{32}F_2$ crystal. Therefore, TiO_2 addition increasing activity values of some main components (CaO, Al_2O_3, and CaF_2) during $Ca_{12}Al_{14}O_{32}F_2$ formation was the main factor in the enhancement of slag crystallization ability with increasing TiO_2 content. This is similar to the role of Li_2O on the crystallization behavior of CaO-SiO_2-based mold flux[25], but different from the effect of TiO_2 on the crystallization behavior of CaO-Al_2O_3-based mold flux when the crystallization behavior of slag is controlled by element diffusion [28]. The morphology of $CaTiO_3$ crystal changed from needle-like to blocky with increasing TiO_2 content. The $CaTiO_3$ crystal with non-faceted morphology indicated that viscosity was the main factor determining the crystallization and the crystallization of $CaTiO_3$ crystal was controlled by the diffusion of species from bulk melts to crystal-melt interface. The MgO crystal was with little blocky morphology, and the CaF_2 crystal with needle-like morphology distributed among $CaTiO_3$ crystal. The precipitated amount of MgO and CaF_2 were both very small, which were in agreement with the DSC results.

3.4 Effective activation energy for crystallization of the slag

The effective activation energy for crystallization is an important parameter to reflect the crystallization tendency of the slag [17,27]. Many methods have been put forward to determine the effective activation energy for non-isothermal crystallization kinetic analysis [29-32]. Friedman method[33], a most widely used method for non-crystallization kinetics analysis during cooling process, was employed to estimate the effective activation energy for crystallization of the slag.

The equation of Friedman method is expressed as follows:

$$\ln\left(\frac{da}{dt}\right) = -\frac{E_{c(a)}}{RT_a} + \text{Const.} \quad (1)$$

where α is crystallization fraction, t, T_α and $E_{c(a)}$ are the crystallization time, the crystallization temperature and the effective activation energy for crystallization at a given crystallization fraction α, respectively.

The crystallization fraction α and its corresponding temperature T_α can be evaluated from the DSC thermal data, as shown in Figure 10. The crystallization fraction α can be obtained by the ratio of A_T/A, where T_O and T_E are the onset temperature and end temperature of exothermic peak, A_T and A are the partial area at the temperature of T_α and the total area of exothermic peak, respectively.

The effective activation energy for $Ca_{12}Al_{14}O_{32}F_2$ crystallization in the slag are presented in Figure 11. It can be seen that there is a notable decrease on the effective activation energy for $Ca_{12}Al_{14}O_{32}F_2$ crystallization with increasing TiO_2 content in the slag, indicating that TiO_2 enhanced the crystallization tendency for the slag to crystallize, which was consistent with the DSC results.

The effective activation energy for $Ca_{12}Al_{14}O_{32}F_2$

crystallization in slag A and B decreased with the increase in the crystallization fraction, and then increased with crystallization fraction. The transition point of these trends approximately corresponds to the crystallization fraction of 0.6 and 0.5 for slag A and slag B, respectively. These results indicate that the crystallization of $Ca_{12}Al_{14}O_{32}F_2$ crystal in slag A and B became easier, and then got harder at the crystallization fraction greater than

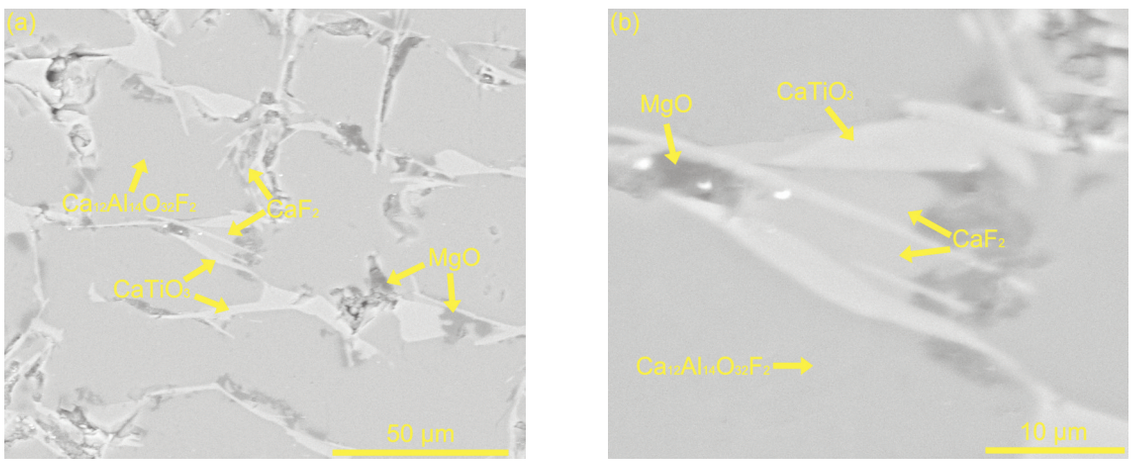

Figure 6. *SEM images of slag A after DSC measurements at the cooling rate of 10 K/min*

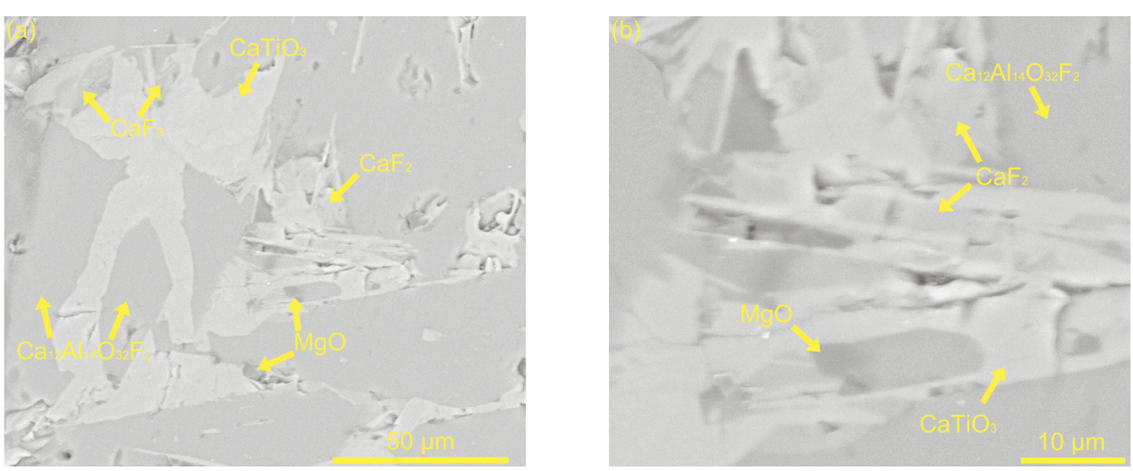

Figure 7. *SEM images of slag B after DSC measurements at the cooling rate of 10 K/min*

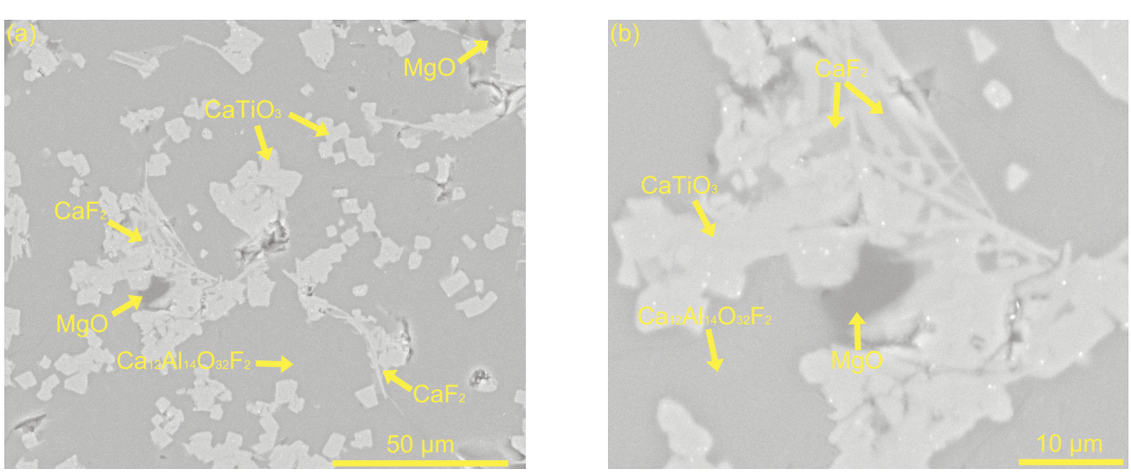

Figure 8. *SEM images of slag C after DSC measurements at the cooling rate of 10 K/min*

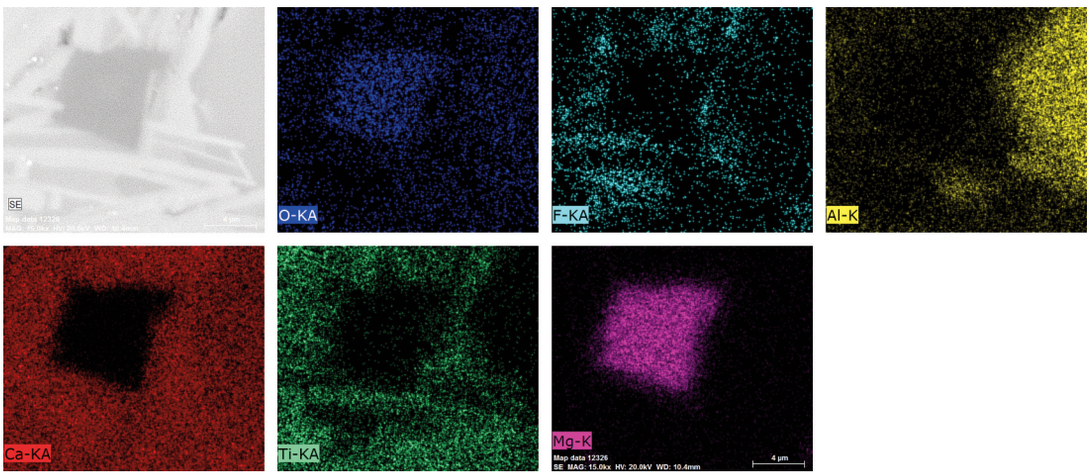

Figure 9. *Element mappings of slag C after DSC measurement*

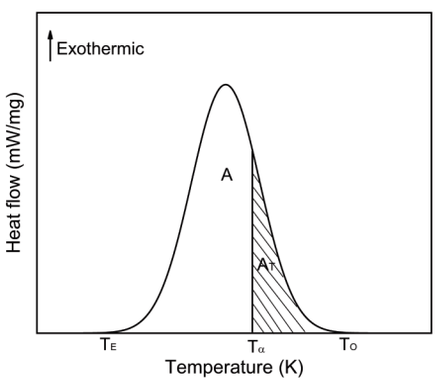

Figure 10. *Schematic of calculation method of crystallization fraction α from the DSC crystallization peak*

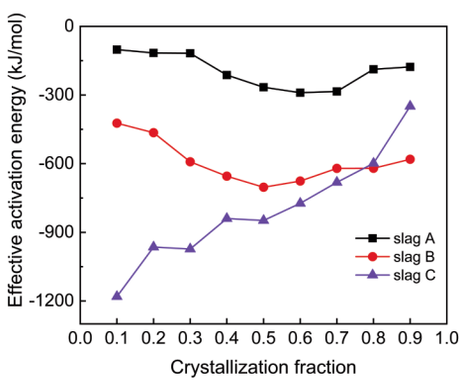

Figure 11. *Dependence of the effective activation energy for crystallization on the crystallization fraction*

0.6 and 0.5 respectively. The effective activation energy for $Ca_{12}Al_{14}O_{32}F_2$ crystallization in slag C increased linearly with the increase of crystallization fraction, suggesting that the $Ca_{12}Al_{14}O_{32}F_2$ crystallization in slag C became harder as the whole crystallization progress.

4. Conclusions

The effect of CaF_2 substitution with TiO_2 on the crystallization characteristics of low-fluoride slag was studied using differential scanning calorimetry (DSC) combined with the XRD and SEM-EDS analysis. The effective activation energy for crystallization of the slag was evaluated. The conclusions are summarized as follows:

(1) The liquidus temperatures of the slag did not have noticeable increase with increasing TiO_2 addition. The undercooling of slag decreased with increasing TiO_2 addition from 4.3 wt% to 13.0 wt%, indicating that the crystallization ability of the slag was enhanced with increasing TiO_2 content in the slag. It is not suitable to substitute excessive TiO_2 for CaF_2 in the low-fluoride slag for electroslag remelting.

(2) There is no change in the types and precipitation sequence of the crystalline phase in the slag with different TiO_2 contents during continuous cooling. The crystalline phases were $Ca_{12}Al_{14}O_{32}F_2$, $CaTiO_3$, MgO, and CaF_2. The first and second crystallization phase were $Ca_{12}Al_{14}O_{32}F_2$ and $CaTiO_3$, respectively.

(3) The dominant crystalline phase in the slag was faceted $Ca_{12}Al_{14}O_{32}F_2$ crystals. The morphology of $CaTiO_3$ crystal changed from needle-like to blocky with increasing TiO_2 content. The MgO crystal formed with little blocky morphology, and the CaF_2 crystal with needle-like morphology distributed among $CaTiO_3$ crystal. The precipitated amount of both MgO and CaF_2 were very small.

(4) The effective activation energy for $Ca_{12}Al_{14}O_{32}F_2$ formation decreased with increasing TiO_2 content in the slag, indicating that TiO_2 enhanced the crystallization tendency of the slag.

Acknowledgments

The financial support by the National Natural Science Foundation of China (Grant No. 51774225) is greatly acknowledged.

References

[1] J. Burja, F. Tehovnik, M. Godec, J. Medved, B. Podgornik, R. Barbič,. J. Min. Metall. Sect. B-Metall., 54 (1) (2018) 53-53.

[2] S.K. Matity, N.B. Ballal, G. Goldhahn, R. Kwaalla, ISIJ Int., 49 (6) (2009) 902-910.

[3] C.B. Shi, H. Wang, J. Li, Metall. Mater. Trans. B, 49 (4) (2018) 1675-1689.

[4] C.B. Shi, W.T. Yu, H. Wang, J. Li, M. Jiang, Metall. Mater. Trans. B, 48 (1) (2017) 146-161.

[5] M. Persson, S. Seetharaman, S. Seetharaman, ISIJ Int., 47 (12) (2007) 1711-1717.

[6] X.F. Zhang, Y. Zhao, Y.G. Hao, Y. Guo, D. Chen, Special Steel Technol., 18 (3) (2012) 38-40. (In Chinese)

[7] D.L. Xiang, Heavy Casting Forging, (2011) 26-35. (In Chinese)

[8] K. Narita, T. Onoye, T. Ishii, T. Kusamichi, Tetsu-to-Hagane, 64 (1978) 1568-1577.

[9] L.K. Liang, G.J. Yue, Z.W. Yue, H. Yang, Journal of Northeast University of Technology., 12 (1991) 230-235.

[10] H.X. Mao, Z. B. Li, Tech. Bull., 3 (1983) 597-611. (In Chinese)

[11] G. Rehak. Proceeding of the 5th International Conference on VM, ESR Processes, Processes, Leybold-Heraeus GMBH, 1976, p. 146-152.

[12] Z.B. Li: Electroslag Metallurgy Theory, Practice, Metallurgical Industry Press, Beijing, China, 2010, p, 45.

[13] Z.B. Li, Steelmaking, 19 (2) (2003) 6-12. (In Chinese)

[14] X.C. Lu, Foundry, 51 (6) (2002) 378-380. (In Chinese)

[15] G. Pateisky, H. Biele, H.J. Fleischer, J. Vac. Sci. Technol., 9 (1972) 1318-1321.

[16] O.A. Sitnikova, S.A. Krasikov, S.A. Istomin, Russian Journal of Non-Ferrous Metals, 53 (6) (2012) 433-436.

[17] Z.Y. Wang, Y.Q. Sun, S. Sridrar, M. Zhang, Z.T. Zhang, Metall. Mater. Trans. B, 48 (1) (2017) 527-537.

[18] A. Shankar, M. Görnerup, A.K. Lahiri, Metall. Mater. Trans. B, 38 (6) (2007) 911-915.

[19] M. Bell, A. Mitchell, J. Iron. Steel. Inst., 209 (1971) 658-670.

[20] C.B. Shi, J. Li, J.W. Cho, F. Jiang, I.H. Jung, Metall. Mater. Trans. B, 46 (5) (2015) 2110-2120.

[21] S. Shi, X. Geng, Z.H. Jiang, H.B. Li, F.H. Xu, L.X. Wang, Chin. J. Eng., 40 (S1) (2018) 47-52. (In Chinese)

[22] C.B. Shi, M.D. Seo, J.W. Cho, S.H. Kim, Metall. Mater. Trans. B, 45 (3) (2014) 1081-1097.

[23] B.X. Lu, K. Chen, W.L. Wang, B.B. Jiang, Metall. Mater. Trans. B, 45 (4) (2014) 1496-1509.

[24] M.D. Seo, C.B. Shi, J.Y. Baek, J.W. Cho, S.H. Kim, Metall. Mater. Trans. B, 46 (5) (2015) 2374-2383.

[25] J.L. Li, Q.F. Shu, X.M. Hou, K.C. Chou, ISIJ Int., 55 (4) (2015) 830-836.

[26] Z.H. Jiang, X. Geng, Adv. Mater. Res., 146-147 (2010) 670-73.

[27] J. Li, W. L. Wang, J. Wei, D.Y. Huang, H. Matsuura, ISIJ Int., 52 (12) (2012) 2220-2225.

[28] M.D. Seo, C.B. Shi, J.W. Cho,, S.H. Kim, Metall. Mater. Trans. B, 45 (5) (2015) 1874-1886.

[29] H.E. Kissinger, Anal. Chem., 29 (1957) 1702-1706.

[30] T. Ozawa, J. Therm. Anal., 2 (1970) 301-324.

[31] K. Matusita, S. Sakk, J. Non-Cryst. Solids, 38-39 (1980) 741-746.

[32] H. S. Chen, J. Non-Cryst. Solids, 27 (1978) 257-263.

[33] H. L. Friedman, J. Polym. Sci. Polym. Symposia, 6 (1) (2010) 183-195.

UTICAJ ZAMENE KALCIJUM-FLORIDA TITANIJUM DIOKSIDOM NA KARAKTERISTIKE KRISTALIZACIJE ŠLJAKE ZA ELEKTRIČNO PRETAPANJE SA NISKIM SADRŽAJEM FLUORIDA

J.-T. Ju *, J.-L An, G.-H. Ji

Metalurški fakultet, Arhitektonsko – tehnološki univerzitet u Šianu, Šian, Kina

Apstrakt

Uticaj zamene kalcijum-florida titanijum dioksidom na karakteristike kristalizacije šljake sa niskim sadržajem fluorida ispitivan je putem diferencijalne skenirajuće kalorimetrije (DSC) u kombinaciji sa XRD i SEM-EDS analizama. Izračunata je i efektivna energija aktivacije potrebna za kristalizaciju šljake. Rezultati su pokazali da se likvidus temperatura šljake neznatno povisila sa povećanjem sadržaja TiO_2. Povećanjem sadržaja TiO_2 sa 4.3 wt% na 13.0 wt%, smanjilo se pothlađivanje šljake i poboljšala se sposobnost kristalizacije. Nisu primećene promene u vrsti i redosledu precipitacije kristalnih faza u šljaci sa različitim sadržajem TiO2 tokom kontinuiranog hlađenja. Dobijene su sledeće kristalne faze: $Ca_{12}Al_{14}O_{32}F_2$, $CaTiO_3$, MgO i CaF_2. Prvu i drugu fazu kristalizacije činili su $Ca_{12}Al_{14}O_{32}F_2$ i $CaTiO_3$. Dominantnu kristalnu fazu činili su kristali $Ca_{12}Al_{14}O_{32}F_2$ sa ravnom površinom. Morfologija CaTiO3 kristala se promenila od igličaste do one oblika blokova prilikom povećanja sadržaja TiO_2. Morfologija MgO kristala je bila u obliku malih blokova, a CaF_2 u obliku iglica koje su bile raspoređene u $CaTiO_3$ kristalu. Nataložena količina MgO i CaF_2 je bila veoma mala. Efektivna energija aktivacije za nastanak $Ca_{12}Al_{14}O_{32}F_2$ se smanjila prilikom povećanja sadržaja TiO_2 u šljaci, što ukazuje da je TiO_2 povećao tendenciju šljake da se kristalizuje.

Ključne reči: *Karakteristike kristalizacije; Šljaka sa niskim sadržajem fluorida; TiO_2; Postupak električnog pretapanja pod šljakom; Efektivna energija aktivacije za kristalizaciju.*